Computers in Biology and Medicine 95 (2018) 63–74

Contents lists available at ScienceDirect

Computers in Biology and Medicine

journal homepage: www.elsevier.com/locate/compbiomed

Effect of off-plane bifurcation angles of primary bronchi on expiratory flows in the human trachea

Youngjoon Suh, Joong Yull Park *

School of Mechanical Engineering, College of Engineering, Chung-Ang University, Seoul, 06974, Republic of Korea

ARTICLE INFO

Keywords:
Off-plane bifurcation
Patient-specific expiratory flow pattern
Rotating airflow in trachea
Three-dimensional human airway geometry

ABSTRACT

Background: The human airway is exposed to the development of diverse flow patterns based on differences in its morphological/geometrical parameters across individuals. Although effects of the asymmetry between the right and left main bronchi on airway flows have been investigated in the past, there exists a paucity in terms of studies that focus on the role of stronger physiological asymmetric features, such as off-plane bifurcation angles of primary bronchi, in expiratory flows.

Method: Computational fluid dynamic techniques have been used to demonstrate presence of Dean-type secondary flows and vortices in the bifurcation region. Formation of a distinctive pattern was observed corresponding to an increase in the off-plane branching angle. An experiment involving 3D printed airways and smoke was also performed to visualize flow patterns and verify simulation results.

Results: Good agreement was observed between computational and experimental results. Furthermore, it was revealed that the predicted wall shear stress distribution demonstrated significant changes (with a maximum shear stress increase of 30.7%) compared to conventional airway models that adopt symmetric bifurcation angles. The overall flow demonstrated a swerving motion, which was characterized by tracking the vortex cores (maximum accumulated radial movement of 72.6°) when they ascended towards the trachea inlet in off-plane airway models.

Conclusions: It was confirmed that off-plane bifurcations in human trachea significantly alter the flow characteristics in expiratory flows. It is expected that the results of this study will provide useful information regarding increasingly advanced patient-specific treatments for respiratory diseases in the trachea.

1. Introduction

Respiratory diseases are being steadily rated as the top cause of fatality in several countries. This is especially caused by the increase in fine dust particles and presence of various viruses in the atmosphere. Results of studies concerning airflow in human airways over the past few decades provide a fundamental step in understanding the onset and development of respiratory diseases, and these have proven as useful in various medical applications concerning respiration [1]. It has also been observed that wall shear stresses developed by respiratory flow modulate the epithelial barrier function of the airway wall; this has an important bearing on wound healing mechanisms [2]. Therefore, it is evident that there is a growing need to better understand and analyze the airflow within human airways. It is also necessary to investigate whether there exist aspects of existing airway flow-prediction studies, which have previously been overlooked, and address them accordingly.

Both experimental and numerical analyses have been performed in the past in order to understand the features and patterns of human-airway flows and aerosol deposition. Experimental studies include studies concerning local deposition efficiencies and patterns of aerosol particles [3] that provide a base to estimate the local deposition dose within an airway. Another experimental study [4] described fundamental flow characteristics, such as secondary flows induced by inspiratory and expiratory flows in symmetric bifurcation models. Computational fluid dynamics (CFD) has also been accepted as a viable tool in studying airway flows whilst being effective in terms of the relative cost and time efficiency. Examples of CFD-based studies that focus on investigation of airway flows include simulation of peak-flow wall shear stresses in the airway [5], particle depositions [6–8], secondary flow patterns [9], and several other topics that have been examined to determine answers for medical inquiries from an engineering perspective. Despite concerns regarding the geometry of the airway model employed in the analyses,

* Corresponding author. School of Mechanical Engineering, College of Engineering, Chung-Ang University, 84 Heukseok-ro, Dongjak-gu, Seoul, 06974, Republic of Korea.
E-mail address: jraprk@cau.ac.kr (J.Y. Park).

https://doi.org/10.1016/j.compbiomed.2018.01.014
Received 29 November 2017; Received in revised form 17 January 2018; Accepted 30 January 2018

0010-4825/© 2018 Elsevier Ltd. All rights reserved.

both experimental and computational methods provide an important platform to understand flows within the human airway.

Extant studies have introduced reliable computational models that yield reasonably good results for researchers better comprehend complex airway flows. Use of simple geometries is effective in order to replicate essential structures within the airway and pinpoint general flow characteristics that occur therein. The symmetric analytic model proposed by Weibel corresponded to one of the first contributions in terms of a systematic quantitative modeling approach applied to trachea bronchus regions [10]. However, studies pointing out the effects of asymmetric aspects of the bronchial system [11,12] have also been performed. These accumulated foundational researches have led to creation of models with new asymmetric features that underline true features of the human airway. Heistracher and Hofmann [13] highlighted the lack of description of the carinal ridge in previous studies and developed a physiologically realistic bifurcation (PRB) geometry based on the Lovelace database [14]. However, the PRB model lacked a mathematical description of the geometry although it closely approximated the shape of the human airway and demonstrated improvement in terms of secondary flow motion over existing narrow and wide bifurcation models [15,16]. Eventually, a model that included a mathematical description of the PRB geometry—the morphologically realistic bifurcation (MRB) model—was proposed [17]. Several researches, since then, have been performed with the objective of developing airway models that comprise larger and complete bronchial geometries [7,18]. As indicated above, extant studies cover several aspects concerning the modeling of airway geometries, respiratory airflow patterns, and particle deposition. However, only very few studies have laid emphasis on the effects of off-plane branching angles on airflows within the human trachea [19,20].

The proposed study presents use of CFD as well as experimental methods to characterize various flow patterns that occur within the human trachea and which are mainly caused by off-plane branching angles. The construction of a typical off-plane bifurcation (OPB) model is illustrated in Fig. 1a. Angles corresponding to 0°, 30°, 60°, and 90° were selected to identify unique flow characteristics that occur at different angles and to determine the flow patterns associated with changes in these angles. Large eddy simulation (LES) and steady laminar models were chosen for the solver. A constant velocity boundary condition of 18 L/min (for simulating the normal respiratory condition in a sitting position [6]) was used in the analysis. Steady-state flow was assumed in order to focus on the investigation of unique flow phenomena caused by variations in off-plane bifurcation angle of primary bronchi. The study reveals how various flow patterns are induced by changing the off-plane bifurcation angle. It is suggested that the effects discussed herein must be accounted for in future studies concerning respiratory flows in human airways.

2. Methods

2.1. Airway geometry

All models were designed and built using a computer-aided design (CAD) software—Autodesk Inventor (Autodesk, Inc. San Rafael, CA, USA). Four models were constructed (Fig. 1b) by preserving the parameters of the PRB model proposed by Farkas and Balashazy [6], as listed in Table 1. The design of each model was performed by drawing curves and

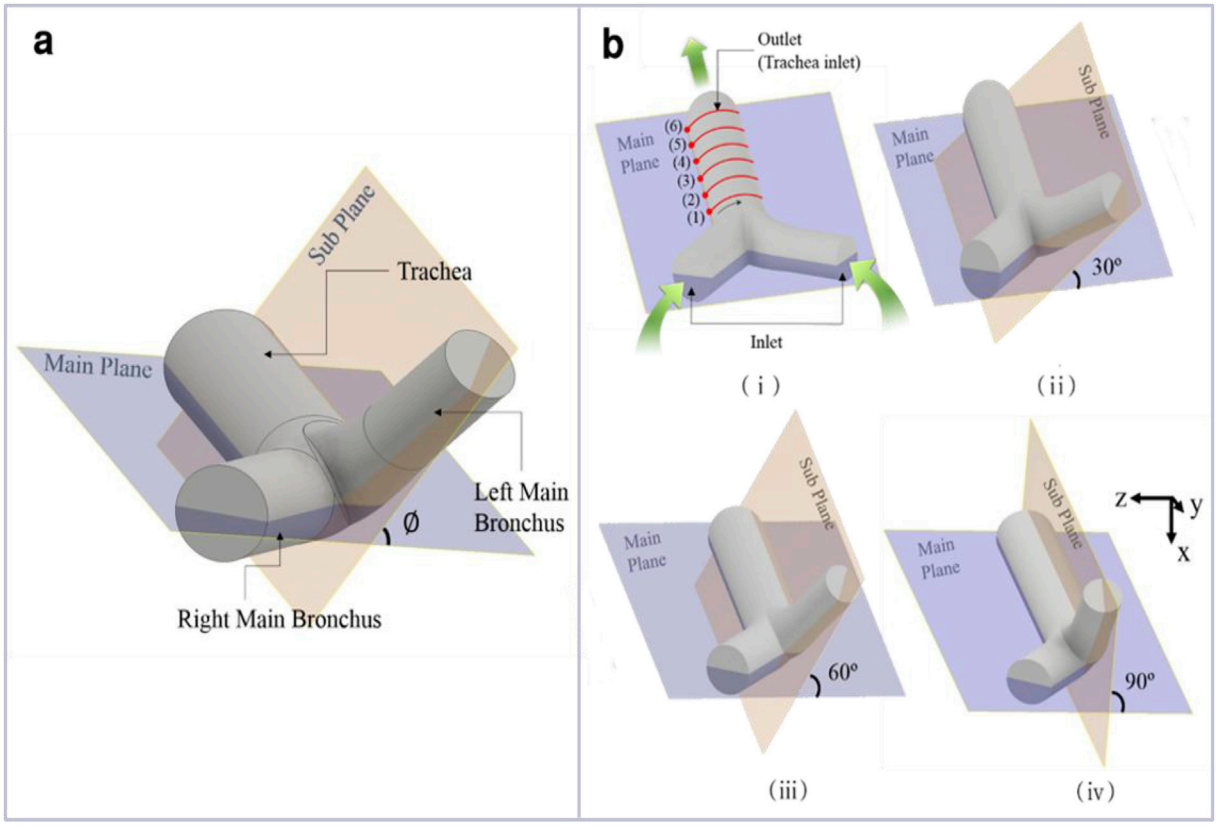

Fig. 1. Airway asymmetry and off-plane bifurcation (OPB) models. (a) Two planes (main and sub planes) were used to construct off-plane bifurcation geometries. The models were constructed using equivalent parameters of the MRB model. The main difference involves generation of the left main bronchus on a sub plane inclined at different angles (Φ). The sub plane angles selected in this study include 0°, 30°, 60°, and 90°. (b) The four OPB models are shown. A velocity boundary condition was defined at the outlet (trachea inlet), and a constant pressure was applied with respect to the two inlets. (i) The model was generated in a symmetric bifurcation plane (OPB-0) by following the procedure listed in most extant studies. Furthermore, the trachea was divided into six sections—(1) to (6)—that indicate locations at which wall shear stresses are analyzed. (ii – iv) The left main bronchus of the model was generated on sub-planes set at angles (Φ) corresponding to (ii) 30° (OPB-30), (iii) 60° (OPB-60), and (iv) 90° (OPB-90).

Table 1
Airway geometry data describing the five bifurcation units of the trachea-bronchial tree. [a]

Gener. no.	L_p [cm]	L_{da} [cm]	L_{db} [cm]	D_p [cm]	D_{da} [cm]	D_{db} [cm]	ϕ_a [°]	ϕ_b [°]	R_a^* [cm]	R_b^* [cm]	R_c^* [cm]
1–2	9.68	1.22	2.15	1.61	1.36	1.10	35	50	3.54	3.54	0.1
2–3	1.22	1.24	0.49	1.36	1.14	0.94	5	85	25.2	1.14	0.1
3–4	0.52	0.72	0.70	0.94	0.83	0.69	45	50	1.14	1.14	0.1
4–5.1	0.72	0.59	0.57	0.69	0.63	0.51	5	45	33.14	3.31	0.1
4–5.2	0.70	0.61	0.59	0.83	0.69	0.63	45	45	1.16	1.16	0.1
Tube no.	1	2	3	4	5	6	7	8	9	10	11
Gravity angle [°]	0	50	35	30	120	108.75	110.7	113.3	67.3	133.1	79.5

[a] L_p is the length of the parent branch, L_{da} and L_{db} are the daughter branch lengths, D_p, D_{da}, and D_{db} are the diameters of the parent and daughter branches respectively, ϕ_a and ϕ_b are maximal sagittal angles, R_a^*, and R_b^* are the curvature radii of the daughter branches and R_c^* is the maximal radius of the carinal rounding.

cross sections onto planes of daughter branches as well as the parent branch (the trachea). Surfaces lying on these curves were created and connected to each other, thereby forming the bifurcation region. Furthermore, off-plane features were explicitly added in the model to retain and depict the three-dimensional (3D) nature of the branching area. In contrast to PRB models, wherein both branches are generated on a single plane, the present model comprises the left main bronchus created on a sub-plane (Fig. 1a). The left main bronchus was sketched at sub-plane angles corresponding to 0° (symmetric geometry), 30°, 60°, and 90° measured with respect to the main plane. The models have been termed "off-plane bifurcation" (OPB) models, and their sub titles are determined based on the angle at which their respective sub planes are inclined, thereby leading to the nomenclature following nomenclature—OPB-0 (symmetric model), OPB-30, OPB-60, and OPB-90. Additionally, domain lengths at the left and right bronchial inlets are set such that they exceed corresponding actual lengths of 2.15 cm and 1.22 cm, respectively, thereby ensuring a fully developed inlet flow. An extension length of L = 15 R is used, where L denotes the extension length and R denotes the primary branch radius [21].

2.2. The computational model

The commercial finite-volume-method (FVM)-based CFD solver package FLUENT 15.0 (ANSYS, Inc., Canonsburg, PA, USA) was employed to obtain numerical solutions for the fluid flow. A velocity boundary condition corresponding to a volumetric flow rate of 18 L/min was applied at the outlet (tracheal inlet; see Fig. 1b) to create a suction effect consistent with the experimental method, and pressure boundary conditions was applied at the inlet (left and right main bronchus). All cases were assumed to include the non-slip boundary condition applied at the walls.

The Reynolds number (Re) is defined by the relation $Re = \rho uD/\mu$, where u denotes the mean flow velocity ($u = 18$ L/min), ρ denotes fluid density ($\rho = 1.2\,kg/m^3$ for air at room temperature), D denotes diameter of the trachea ($D = 1.6$ cm), and μ denotes dynamic viscosity ($\mu = 1.82 \times 10^{-5}\,N\,s/m^2$ for air at room temperature). The room temperature, measuring 22 °C, was used to compare results with those obtained from flow-visualization experiments performed at room temperature. A previous study [22] demonstrated that the temperature of the breath exhaled by a human ranges from 32.29 to 35.84 °C (mean = 34.84 °C). The viscosity of air at 35 °C is about $1.88 \times 10^{-5}\,N\,s/m^2$, which is little higher (3%) than the value used in the simulations.

The corresponding flow exhibits Re of the order of 1400, and is, therefore, considered as being laminar. Nevertheless, a transient turbulence model (LES) was chosen as a precaution against turbulent eddies induced owing to geometric influences [22,23]. The Smagorinsky–Lilly model was selected in this study. The results obtained using the LES model were compared with those obtained using the steady laminar model, and minor differences (see Fig. S1) were observed.

2.3. The computational grid

The ANSYS ICEM CFD software was used to generate the computational grid upon which the numerical simulations were performed. ICEM CFD is a grid-generation package based on CAD, and supports generation of multiblock structured, unstructured tetrahedral, and hexahedral grids. An unstructured grid comprising hexahedral elements throughout was constructed using blocking tools available within ICEM, as depicted in Fig. 2. The classical method employing the butterfly topology was not used to create hexahedral meshes for use in this study. Instead, two blocks were combined to create a hexagon-shaped O-grid in order to enhance meshing quality in regions closer to the wall. O-grid pre-mesh parameters were used to define a "size function" to ensure that the mesh in near-wall regions was dense enough to accurately capture the flow boundary layer. Because of the relative concavity of the hexagonal O-grid, it was possible to generate a mesh comprising lesser cells with more accurate computational processing. The mesh size in each model was determined by increasing the scale factor of the mesh until incremented meshes and calculated values of the previous mesh exhibited a tolerance of approximately 0.5% (see Fig. S2). The flow velocity was measured and plotted from the bottom of the model to its top or from the

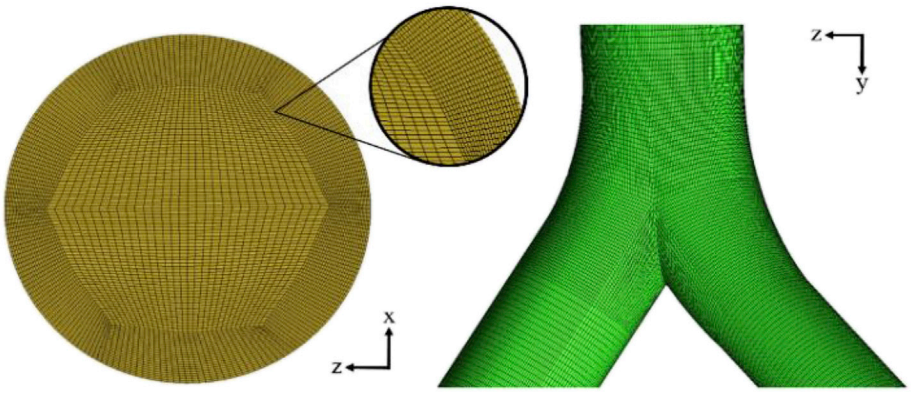

Fig. 2. The computational grid of the trachea cross-section (*left*) and surface mesh (*right*) corresponding to the OPB-60 model with a mesh element count of approximately 3 million. The area near the wall has been magnified to provide detailed insight into mesh sizing. This type of a fine grid near the wall is necessary for the accurate estimation of wall shear stresses.

bifurcation zone to the tracheal inlet. The average mesh-element count approximately corresponded to 2×10^6.

2.4. Experimental setup for the airway model

OPB-0, OPB-60, and OPB-90 models were printed using 1.75 mm acrylonitrile butadiene styrene (ABS) 3D filament by means of a 3D printer (3DP-210F, HyVision, Cubicon, Republic of Korea). A glass tube was inserted into the observation area to visualize cross-sectional airflow inside the airway model. A schematic of the experimental setup for the airway is depicted in Fig. 3. Smoke was generated by sublimating 2 dry ice cubes—one each for the left and right main bronchi. A constant suction flow of 18 L/min was generated at the inlet to the model, and smoke movement was visualized by means of an endoscope (MSIP-REI-1js-HD-Camera, DOYAMA, Φ 5.5 mm, China) located in the mid-section of the trachea, approximately 4 cm above the observation area, to achieve optimized resolution. The endoscope was fixed by means of a 3D-printed endoscope fixation connecter. The green laser diode (PT Time, Class HIB laser line generator, Seoul, Republic of Korea) used during experiments exhibited a wavelength of 32 ± 5 nm and a generating capacity of 50 mW.

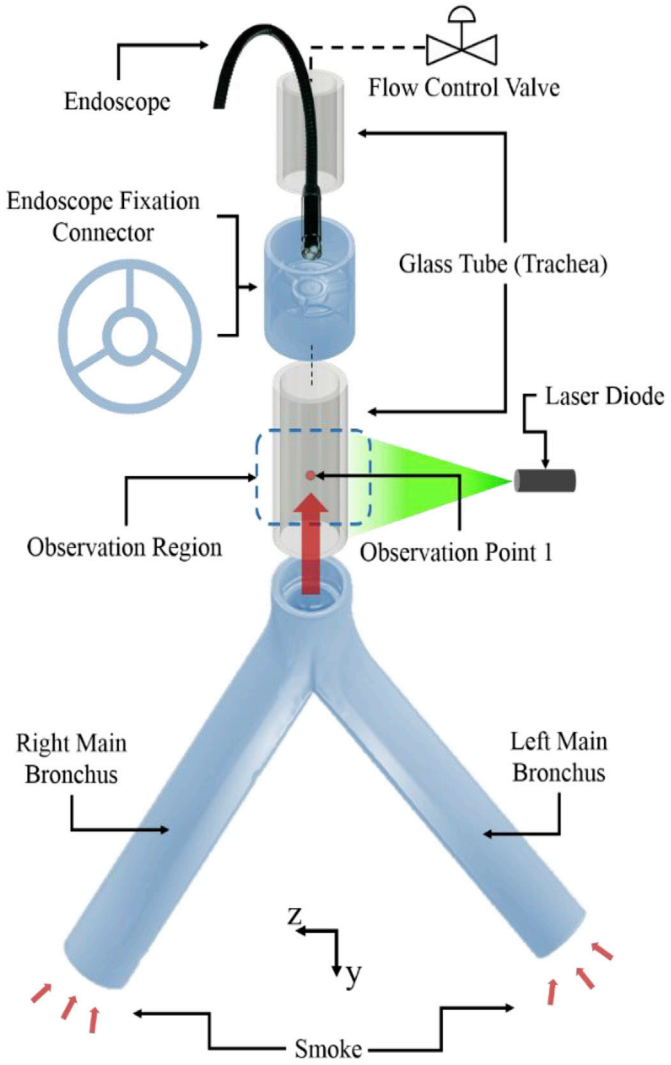

Fig. 3. Schematic of the experimental setup employing the proposed airway model, OPB-60. The model was designed such that a glass tube could fit inside 3D-printed left and right main bronchi having thickness corresponding to that of the tube. Visualization range of the endoscope was limited to approximately 40 mm. Thus, the endoscope was stationed at a location approximately 40 mm above the PVC tube in order to obtain optimized visual resolution. Observation point 1 was located 7.7 cm upstream of the model outlet (trachea inlet), and the same location was used for CFD analysis, as shown in Fig. 4. The laser sheet generator diode enabled smoke visualization inside a dark room. The smoke was generated by sublimating dry ice cubes placed inside two $20 \times 20 \times 20$ cm acrylic boxes where the boxes corresponded to the left and right main bronchi. The flow rate was controlled using a flow-control valve located at the trachea inlet.

3. Results

3.1. Characteristics of vortex formations at the bifurcation

The presence of Dean-type secondary flow patterns [24] was found to be prominent in each model. Vortices were generated across a cross-sectional plane (analogous to the observation location considered during experiments) in the vicinity of the bifurcation (Fig. 4). Four vortices were created owing to the radial pressure gradient and centrifugal force imbalance, and this corresponded to a representative secondary flow pattern of the Dean type. The flow pattern was represented by tangentially projected streamlines and velocity vectors (Fig. 4a). Each vortex core was marked manually and identified as a dot. The vortex cores were observed to have originated in the bottom-left corner and were labelled in the clockwise sense as C1, C2, C3, and C4. The cores were grouped based on their respective coordinates (Fig. 4b), and their corresponding forming tendencies were compared for each different branching angle. The results indicate that the vortex cores exhibited a distinct formation pattern, which was highly dependent on the angle and location of the left and right main bronchi. In Fig. 4c, the four OPB models are gathered and aligned such that the viewer can visualize the manner in which branching angles were generated. The left main bronchus was positioned horizontally to establish a standard reference position for comparison of the orientation of the right main bronchus. A plot of the distance between each vortex core in each OPB model is depicted in Fig. 4d. The distance between vortex cores C1 and C2 displays very low inconsistency for each model with an average distance of 4.85 mm and a standard deviation of 0.29 mm. With increase in branching angle from 0° to 90° (OPB-0 to OPB-90), the distance between vortex cores C2 and C3 exhibits a steady decrease with an average length of 1.45 mm while that between cores C3 and C4 demonstrates an increase. The distance between vortex cores C1 and C4 exhibits a linear increase with the bifurcation angle with an average length of 0.77 mm. It is also observed that the equal spacing between vortex cores C1 and C2 does not change, although it is shifted downwards by the secondary flows corresponding to cores C3 and C4.

3.2. Comparison of experimental and numerical flow patterns at the bifurcation

The experimental results were found match reasonably well with corresponding numerical predictions (Fig. 5). The vortex cores were considered as suitable parameters for flow-profile analysis and were closely observed. Experimental results (*left,* Fig. 5) for secondary-flow motion (vortices) at the observation point 1 (Fig. 3) were compared with results obtained via CFD (*right,* Fig. 5) simulations. Despite the fluctuating flow, four extremely clear vortex motions were observed in the OPB-0 model (Fig. 5a), wherein the vortex cores generated on the right and left sides were of nearly equal sizes owing to symmetric features of the OPB-0 model. Dean-type flow characteristics in the OPB-60 model (Fig. 5b) were also observed to be consistent with numerical data acquired via CFD. The vortex cores demonstrated a tendency to veer in a direction corresponding to the angle of the main bronchus. Furthermore, the two vortex cores induced by the left bronchus (C1 and C2) were observed to have shifted to a lower position owing to counterclockwise movement of the two vortices on the right. Finally, the OPB-90 model (Fig. 5c) was observed, and the secondary-flow motion therein was also found to induce counterclockwise changes in vortex-core locations.

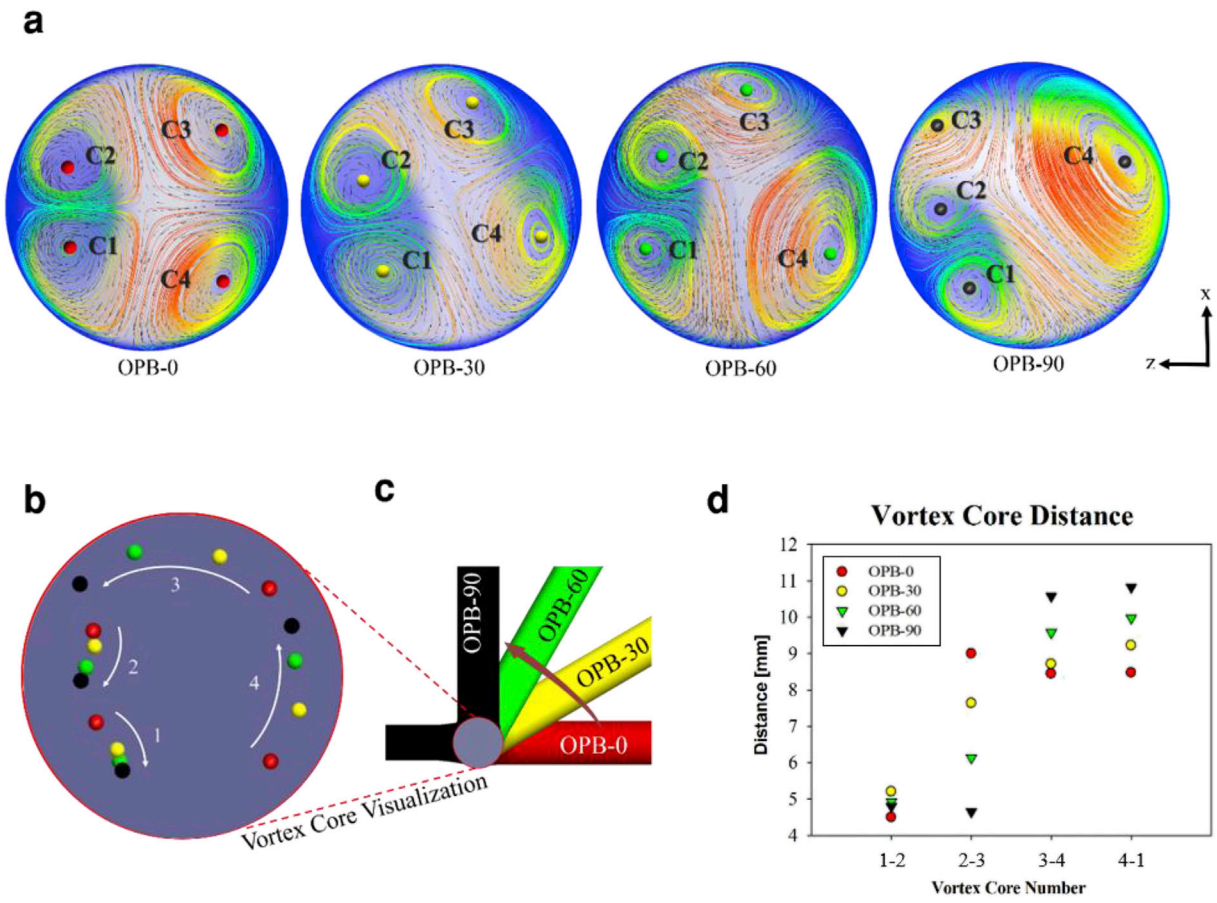

Fig. 4. Distinctive pattern of vortex cores developed owing to variations in the branching angle of the main bronchi. (a) Development of individual vortex core models. The vortex cores are identified by numbers, the lowest being assigned to the bottom left core for a more in-depth identification of its development and patterns. (b) Vortex cores in each model were aggregated onto a circular plane, which corresponded to the observation plane near the bifurcation. The arrows represent coordinate changes in vortex cores C1–C4 with respect to changes in sub-plane angles. The dots are denoted as red, yellow, green, and black to represent models OPB-0, OPB-30, OPB-60, and OPB 90, respectively. (c) In order to ensure that the viewer obtains a better understanding of the flow characteristics in (a) and (b), the four OPB models are aligned in the same coordinate form. (d) A plot of the distance between each vortex core in the OPB-0, OPB-30, OPB-60, and OPB-90 models. Each model represents a different color and symbol where OPB-0, OPB-30, OPB-60, and OPB-90 correspond to red (circle), yellow (circle), green (triangle), and black (triangle), respectively. The two Dean-flow originated vortices generated from the left main bronchus gap correspond to vortex cores C1 and C2. It is observed that the distance between these cores displays high consistency, while the vortex core pair in the right main bronchus, namely C3 and C4, exhibit a gradual increase in distance. Furthermore, the distances between cores C2–C3 and C4–C1 exhibit linearity in their shifts in position. (For interpretation of the references to color in this figure legend, the reader is referred to the Web version of this article.)

3.3. Flow development in the tracheal region

Secondary flows, when developed up to the inlet of the trachea, were observed to exhibit a slight swerving motion. This section emphasizes on three key points—the counter-clockwise swerving motion of the flow when it escalates up towards the trachea inlet, presence of a dominant vortex on account of flow three-dimensionality, and the region wherein highly complicated flows begin to appear. It is illustrated that an overall scheme of expiratory flow disposition as the flow escalates in Fig. 6. The trachea was divided into six regions (similar to Fig. 1b) beginning with observation point 1 (Fig. 3).

The flow began to display swerving motion as it escalated up towards the trachea inlet (between locations 1 and 6) when the models was introduced to out-of-plane bifurcation angles. As observed in the OPB-0 case, the four secondary flow vortex cores were seen to join together without generation of any additional observable secondary flows. In contrast, in cases OPB-30, OPB-60, and OPB-90, the vortex cores began to rotate in the counter-clockwise direction whilst moving towards the center of the airway. The swerving fluid motion in the off-plane models began to attenuate as the flow ascended towards the upper-trachea, and complex flow patterns began developing (Fig. 6b). The said swerving motion of the fluid was analyzed by tracking the radial movement of the vortex cores (Fig. 7a and b). The counter-clockwise (CCW) direction was defined as positive while measuring the angles of rotation. The graph (Fig. 7b) on which the accumulated angle of each core was plotted was used as an indicator of the radial movement of the cores. In the OPB-0 model, discrepancies between the absolute values of C1 and C2 (3.5%) as well as C3 and C4 (5.2%) were the fund to be the lowest. The maximum accumulated radial movement of the C4 vortex was observed to be 72.6° in the OPB-90 model. Furthermore, the distance between each core and the origin was tracked and plotted (Fig. 7c and d) as the flow began to ascend towards the trachea inlet. The variation of the total distance is listed in Table 2.

Additionally, the presence of dominant vortex cores was observed. By identifying the vortices by numbers, as described in Fig. 4, vortices C1 and C4 were observed as being dominant. When the branching angle was set to 90° (OPB-90 model), the dominant cores began to play a significant role in flow distribution. Strength of the dominant cores was based on the swirling-strength criterion, which represents the strength of the local swirling motion and corresponds to the imaginary part of complex eigenvalues of the velocity-gradient tensor [25,26]. The concerned theory is based on the concept of decomposition of the velocity-gradient tensor,

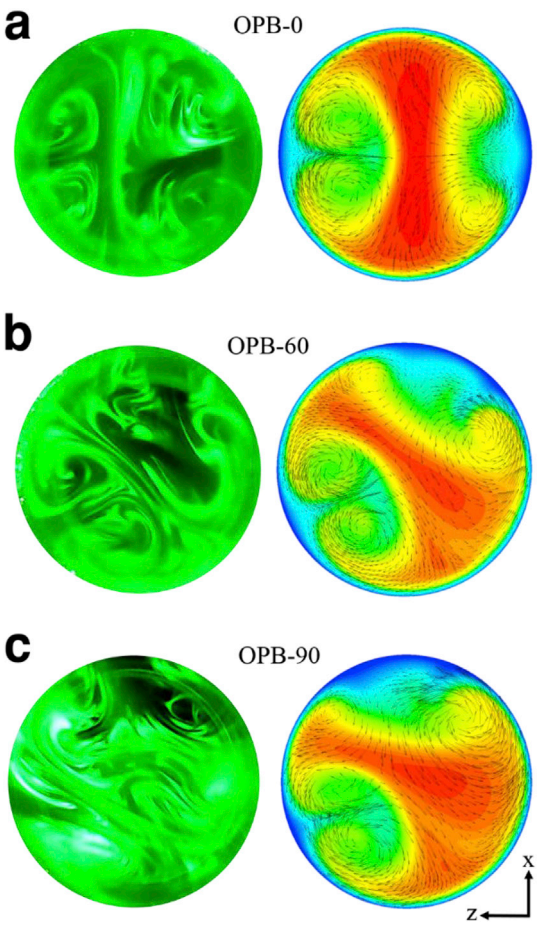

Fig. 5. Comparison of experimentally procured results with results obtained from numerical simulations. The purpose of the experiments involved verifying the formation of vortex cores in extreme cases, such as OPB-60 and OPB-90. Additionally, OPB-0 has been included to demonstrate the formation of secondary flow-induced vortex cores in symmetric bifurcation plane angles (as used in most extant studies). In all the cases, four vortex cores were generated by the Dean-type secondary flow. The two vortex cores on the left side are developed owing to the imbalance in radial pressure gradients and centrifugal force of the left main bronchus, while the two cores on the right represent products of corresponding imbalances induced by the right main bronchus. (a) Experimental and numerical results for the symmetrically branched model, OPB-0, are compared. The presence of four vortex cores is very clear and easy to observe. (b, c) Vortex cores in out-of-plane bifurcation models are also observed at agreeable locations.

∇u, in Cartesian coordinates and can be mathematically represented as

$$\nabla u = [d_{ij}] = [\,\overline{\nu}_r \quad \overline{\nu}_{cr} \quad \overline{\nu}_{ci}\,] \begin{bmatrix} \lambda_r & & \\ & \lambda_{cr} & \lambda_{ci} \\ & -\lambda_{ci} & \lambda_{cr} \end{bmatrix} [\,\overline{\nu}_r \quad \overline{\nu}_{cr} \quad \overline{\nu}_{ci}\,]^T \tag{1}$$

Where d_{ij} represents the velocity-gradient tensor in Cartesian coordinates, λ_r is the real eigenvalue of the corresponding eigenvector v_r. The complex eigenvectors $v_{cr} \pm v_{ci}i$ comprise conjugate pairs of eigenvalues given by $\lambda_{cr} \pm \lambda_{cr}\, i$. The local streamlines could be expressed as

$$y_1(t) = C_r \exp \lambda_r t \tag{2}$$

$$y_2(t) = \exp \lambda_{cr} t \left[C_c^{(1)} \cos(\lambda_{ci} t) + C_c^{(2)} \sin(\lambda_{ci} t)\right] \tag{3}$$

$$y_2(t) = \exp \lambda_{cr} t \left[C_c^{(2)} \cos(\lambda_{ci} t) + C_c^{(1)} \sin(\lambda_{ci} t)\right] \tag{4}$$

in the local coordinate system defined by three vectors (v_r, v_{cr}, v_{ci}). In the above equations, C_r, $C_c^{(1)}$, and $C_c^{(2)}$ are constants. With the establishment of the above mathematical concept, the fluid was found to demonstrate swirling motion on the plane spanned by the vectors v_{cr} and v_{ci}. The imaginary part of the complex eigenvalue pair (λ_r) was referred to as the swirling strength, and in ANSYS CFD-Post, it is defined as the magnitude of both, the "swirling vector" and "swirling normal".

Table 3 summarizes variations in the swirling strength of the vector in each vortex core corresponding to locations 1–6 depicted in Fig. 6a. Individual vortex cores were identified by numbers, as described in Fig. 4. As expected, no distinguishable dominant cores were observed in the OPB-0 model. However, the emergence of such cores began was observed in the OPB-30, OPB-60, and OPB-90 models. Furthermore, in the OPB-30 and OPB-60 models, vortices C2 and C4 were observed to emerge as dominant cores in terms of their respective swirling strengths. In all the off-plane model, the C4 vortex was found to remain steady as the dominant vortex core on the right side. The four vortices in the OPB-90 model were observed to have eventually forged into two dominant cores, namely C1 and C4, while C2 and C3 were seen to gradually attenuate and disappear. With the exception of the symmetric model (OPB-0), all 3D models demonstrated existence of C4 as the dominant core.

3.4. Shear stress

An analysis of the wall shear stress was performed (Fig. 8a–d) to observe the effect of shifting flows on the tracheal wall. Data concerning the shear stress profile were calculated around the circumference of the bronchus wall when the flow was found to rise towards the outlet (locations 1–4, as depicted in Fig. 1b). The locations of measurement were equivalent to those depicted in Fig. 6a. The direction of the circumference was considered clockwise starting from the right tracheal wall. The measured shear stress profiles demonstrated a shift in their formation with variations in the 3D off-plane branching angles. The shear-stress profile corresponding to the OPB-0 model (Fig. 8a) does not demonstrate any shift in shear-stress formation. Conversely, shear-stress profiles corresponding to all remaining off-plane models demonstrated an overall shift towards the right (Fig. 8b–d), the shift became more evident with increase in the branching angle. Further, shear stresses on the anterior (approximately 40°–140°) and posterior (approximately 200°–300°) sides of the airway also exhibited varied amounts of shifting. The total shift in shear stress on the posterior side of the trachea was found to exceed that on the anterior side.

Additionally, the overall asymmetric features of the geometry were found to alter the range and pattern of resulting wall shear stresses. When compared to the OPB-0 model, it was observed that an enhanced maximum shear stress was applied on the tracheal wall, to a small extent, in other models. As expected, location 1 in the vicinity of the bifurcation was found to demonstrate the highest shear stress levels. A maximum shear stress of 0.075 Pa was observed in the symmetric model (Fig. 8a). This value was found to increase by 30.7%, 26.7%, and 12.0% in the OPB-30, OPB-60, and OPB-90 models, respectively. Furthermore, shear stress disposition on the posterior wall of the trachea was found to expand with increase in off-plane branching angles.

4. Discussion

4.1. Flow characteristics of off-plane bifurcation (OPB) airway geometries

Generally, the right main bronchus of the human airway is thicker and produces higher mass flow during exhalation when compared to the left main bronchus. The ratio of flow partition between the left and right main bronchi, in this study, approximately corresponded to 4:6. Previous studies did not examine the effect of this flow mismatch in off-plane airway geometries (OPB-30, 60, 90) in much detail. It is speculated that imbalanced exhalation flow characteristics of the left and right main bronchi are amplified in off-plane airway geometries. This leads to concentration of the flow in the posterior of the airway, eventually

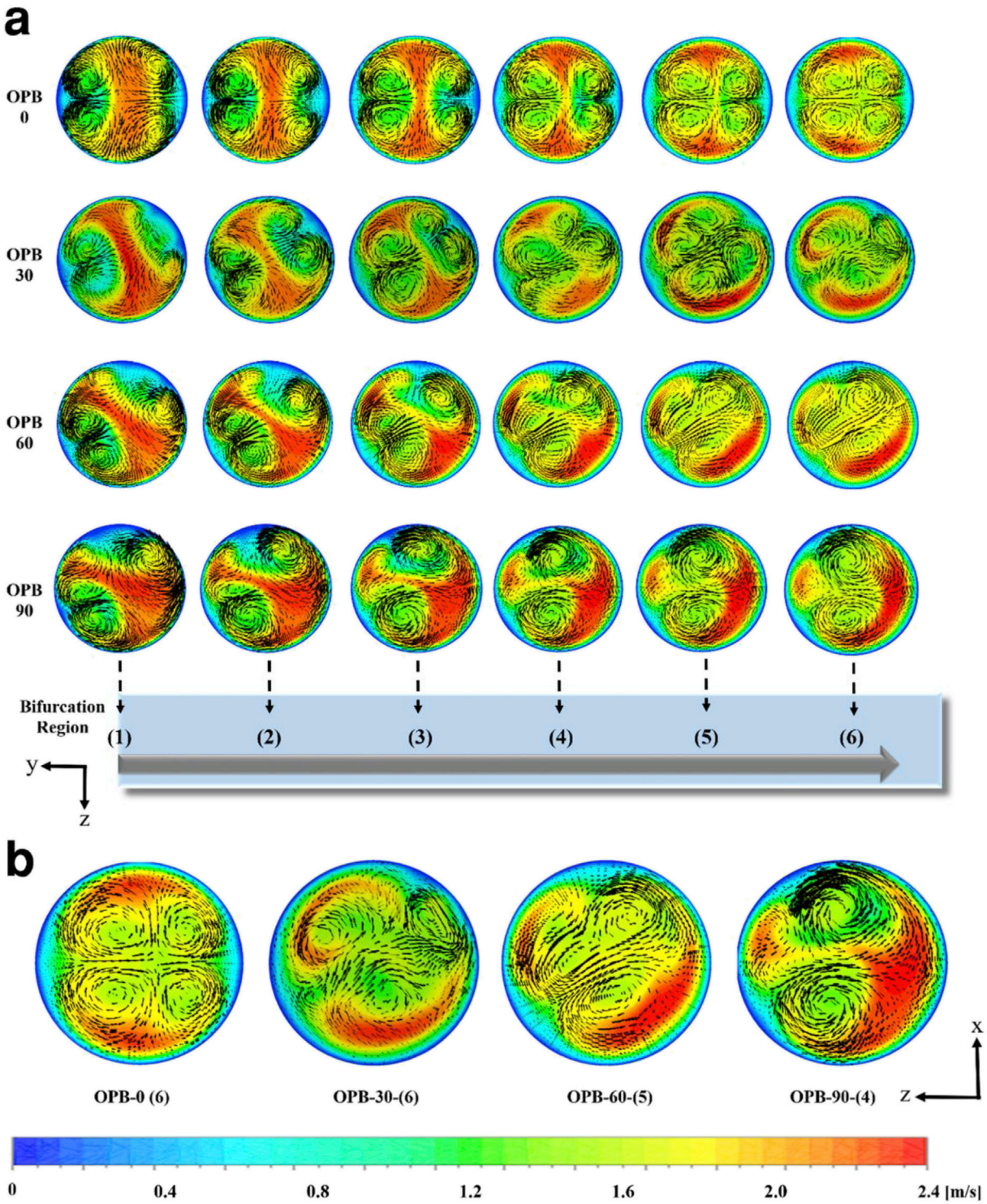

Fig. 6. Flow development in the trachea. (a) The expiratory flow was observed as it develops near the inlet of the trachea for every OPB case. Each model was visualized in coordinate frames equivalent to those in Fig. 5, wherein the left main bronchus is located on the left of the picture while position of the right main bronchus changes with variations in the 3D bifurcation angle of the model. Six observation locations (equivalent to the six locations in Fig. 1c) were considered. Location 1 corresponds to the cross-sectional area nearest to the bifurcation region. Furthermore, the locations mentioned refer to those displayed in the above figure. In all models, with the exception of the OPB-0 model, a counter clockwise rotating development of secondary flow was observed. The presence of dominant cores cannot be predicted from the above picture because the difference between swirl strengths of the cores is not significant. However, the dominance of the C4 vortex core (as depicted in Fig. 4a) manifests itself in OPB-30, OPB-60, and OPB-90 models. (b) The flow field has been magnified in areas wherein complex flows begin to appear. The numbers assigned to model names correspond to locations (*top,* Fig. 6a or in Fig. 1c) at which the cross-sectional pictures have been captured. Furthermore, OPB-0 does not display any significant signs of complex flows even at location 6. Complex flows begin to develop in the upper trachea at the instant when attenuation of the expiratory flow diminishes geometrical effects onto the secondary flow.

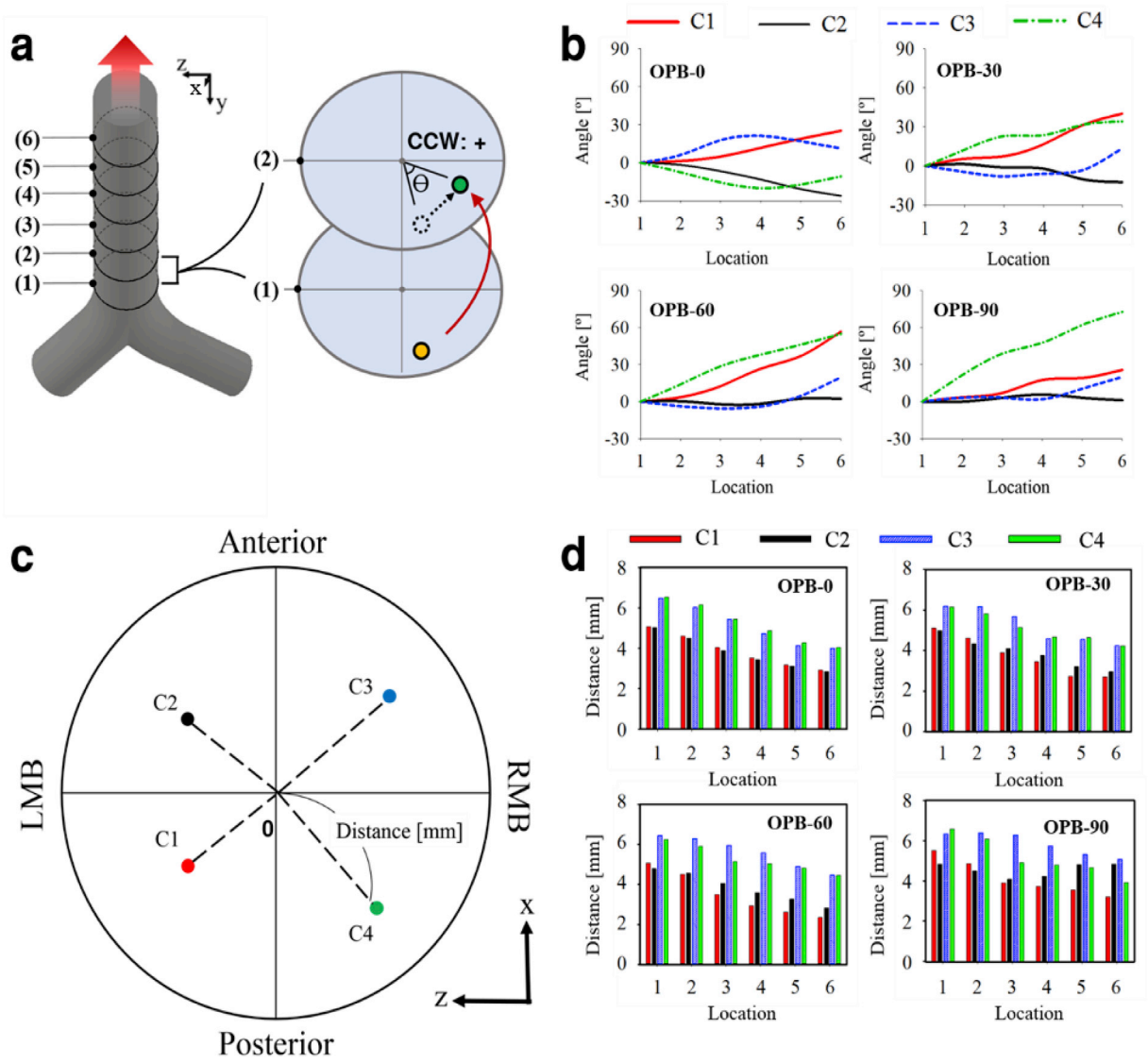

Fig. 7. Coordinate movement tracking of vortex cores during the expiratory flow. Angular motion of the four vortex cores (C1–C4) in each OPB model has been tracked and plotted. Furthermore, the distance between each core and the origin of the cross-section is plotted to determine how the vortices conjure when the flow proceeds toward the trachea inlet. (a) A figure depicting locations 1–6. The illustration (*left,* a) is an example of how vortex-core movement angles are defined and shows the magnified cross-sectional plane at locations 1 and 2. The core that develops in location 1 (yellow circle) swerves in the counter-clockwise direction when it develops towards location 2 (green circle). The angle that is created between the vortex core at locations 1 and 2 corresponds to θ. The counter-clockwise direction is defined as positive for the swerving motion. (b) The accumulated angles (radial movement) of the vortex cores when the flow ascends from location 6 to 1 are plotted for each OPB model. The cores are denoted by individual colors and patterns as follows: C1 (red, solid line), C2 (black, solid line), C3 (blue, dotted line), and C4 (green, dotted line). (c) A cross-section is visualized for the viewer to appreciate the manner in which the distance from individual cores to the origin are determined. The position of the left and right main bronchi (LMB and RMB, respectively), with addition of the anterior and posterior sides of the trachea, is included for the sake of clarity. Four examples of vortex cores are provided with their respective colors (C1, C2, C3, and C4 denoted in red, black, blue, and green, respectively) corresponding to the legends used in this figure. (d) The distance from each core to the origin is plotted. The locations correspond to those demonstrated in (Figs. 1c, 6a and 7a). (For interpretation of the references to color in this figure legend, the reader is referred to the Web version of this article.)

Table 2
Changes in the total distance from the vortex core to the origin.

Model	OPB-0	OPB-30	OPB-60	OPB-90
Vortex Core	Total Distance Decrease from Core to Origin [%]			
C-1	42.6	47.1	53.7	41.7
C-2	43.0	40.6	40.9	0.21
C-3	38.4	31.5	30.8	20.3
C-4	38.1	31.2	28.8	40.3

causing it to develop distinctive flow features. Difference in flow characteristics between symmetric and off-plane geometries evidently provide new pathological interpretations of the airflow related to human exhalation.

As discussed in the foregoing analysis, formation characteristics of quadruple vortex cores in the exhalation flow demonstrated significant changes at off-plane bifurcation angles. In the case of a symmetrical bifurcation airway geometry (OPB-0), flow from each daughter branch was found to converge at the center of the trachea and subsequently diverge away from the center to form the four vortex cores (Fig. 4). The flow tends to diverge towards the anterior and posterior walls in relatively equal proportions. In accordance with Bernoulli's principle, when the flow meets the anterior and posterior walls (stagnation points), the fluid velocity decreases, thereby causing an increase in the static

Table 3
Description of the swirling strength of the vortex cores.

Model		OPB-0	OPB-30	OPB-60	OPB-90
Observation Location	Vortex Core	Vector Swirling Strength [s^{-1}]			
Location 1	C-1	406.5	556.9	532.6	450.3
	C-2	412.0	608.6	756.3	520.1
	C-3	368.8	377.3	248.9	195.0
	C-4	361.1	637.6	634.6	493.9
Location 2	C-1	348.1	459.0	430.6	367.7
	C-2	348.8	477.1	630.0	398.3
	C-3	319.2	355.6	223.1	179.3
	C-4	317.1	540.9	621.0	528.5
Location 3	C-1	276.7	352.8	336.8	301.9
	C-2	277.0	422.7	494.4	237.5
	C-3	279.1	293.3	225.8	153.8
	C-4	259.0	446.3	476.4	450.1
Location 4	C-1	232.5	349.1	297.1	273.0
	C-2	233.5	358.3	408.2	N/A[a]
	C-3	232.3	254.2	182.3	141.3
	C-4	228.2	344.5	398.2	356.1
Location 5	C-1	206.2	251.9	256.2	243.4
	C-2	207.7	320.7	336.6	N/A
	C-3	203.5	214.7	N/A	N/A
	C-4	198.9	348.8	342.2	297.7
Location 6	C-1	190.0	275.7	232.4	222.3
	C-2	191.0	304.1	278.2	N/A
	C-3	182.0	206.6	N/A	N/A
	C-4	179.6	280.5	298.5	262.9

[a] Vortex cores that were indistinguishable were marked as 'N/A'.

pressure. Therefore, increased pressure distributions are generated at the anterior and posterior walls with a slight bias towards the left (Fig. 9a), since the flow from the right main bronchus is comparatively stronger. The resulting fluctuating flows in these locations cause a stronger swirl (vortex), and thus, the C1 and C2 vortex cores (Table 3) become dominant in the bifurcation region. However, in cases wherein the bifurcation is off-plane, the fluid flow exhibits a bias towards the posterior region (Fig. 9b–d). An increase in the pressure distribution in the posterior region leads to development of the C4 vortex core, which later develops into the dominant vortex core in off-plane geometries.

Increased flow concentration—which induces higher static pressure distribution—near the posterior wall also influences wall shear stress distribution characteristics. The OPB-0 model (Fig. 8a) exhibits almost identical shear stress distributions on the anterior and posterior walls, while corresponding wall shear stress distributions in off-plane airway geometries (Fig. 8b–d) are found to gradually spread. Such distributions are attributed to initial locations of vortex cores in the bifurcation region (Figs. 4–6). An increase in the distance between cores C1 and C4 leads to expansion of the range over which the flow remains concentrated at the posterior wall. Additionally, for all off-plane bifurcation models, results of the proposed study yielded higher shear stress levels when compared to those observed in the OPB-0 model. This indicates that the overall micro-scale airway environment is altered in off-plane bifurcation geometries. This implies that wall shear stress values reported in extant studies, involving modeling and utilization of symmetric bifurcation plane angles, may not match those generated inside a typical human airway. This highlights the need for a new pathological interpretation base.

The exhalation flow has been found display counter-clockwise swerving motion as it develops towards the outlet of the airway (Fig. 6). It is also speculated that this swirling motion, which, by the way, is only found in the off-plane bifurcation models (OPB-30, 60, and 90) is generated by a combination of off-plane flow paths, increased concentration of the flow in posterior regions, and dominant mass flow from the right main bronchus. This belief is bolstered by examination of the radial movement of the vortex cores, as depicted in Fig. 7b. In the OPB-0 model, vortex cores C1 and C3 exhibit movement in the counter-clockwise direction while C2 and C4 exhibit clockwise movement. Angular movements of the four cores were found to be symmetric. Adversely, however, swirling motion of the vortex cores was conspicuous in the out-of-plane bifurcation models (OPB-30, OPB-60, and OPB-90). In these models, the clockwise motion of the vortex cores was found to have been significantly reduced while the counter-clockwise motion demonstrated an increase as the flow was elevated (from location 1 to 6). Furthermore, vortex cores C1 and C4 (generated in the posterior region) demonstrated a significantly higher degree of counter-clockwise movement compared to C2 and C3. The aforementioned results imply that the counter-clockwise swerving motion of the flow was influenced more by vortex cores C1 and C4 positioned near the posterior region as opposed to cores C2 and C3. Furthermore, examination of the overall rightward shift of the wall shear distribution plot (Fig. 8b–d) also leads to the same conclusion. To the best of the authors' knowledge, the swerving motion of the developing exhalation flow is a newly discovered phenomenon that is potentially linked with the change in wall shear distribution as well as the maximum shear stress that cells may be subjected to in a micro-scale environment. A better understanding of this phenomenon could play a crucial role in determining a solution for unresolved respiration-related inquiries. It must, however, be noted that such swerving motions are not adequately depicted in conventional (on-plane) symmetric airway models, and thus, off-plane geometric effects on expiratory flows inside the airway must be accounted for to ensure further improvements in CFD-assisted airway diagnostics.

Shear stress distributions on the tracheal wall could be clearly seen to be correlated with off-plane bifurcation angles of the airway (Fig. 8). As mentioned in the Introduction section, a previous study quantitatively demonstrated that airway epithelial cells respond to shear stresses generated by the airflow. It may, therefore, be inferred that shear stresses bear a quantitative relationship with epithelial cell permeability (inversely) and play a significant role in improving the epithelial barrier function [2]. This implies that a more precise prediction of shear stress distributions within airways would be beneficial in understanding wound-healing mechanisms of respiratory epithelia. Therefore, future studies on bronchial flows must be performed with the open idea of accounting for the effects of morphological characteristics of three-dimensionally bifurcated airways on the resulting flow.

4.2. Numerical solver

Extant studies prescribe several options in terms of the numerical methodology to be used given the complex geometry of an airway. The three most popular models include, direct numerical simulation (DNS), large-eddy simulation (LES), and Reynolds-averaged Navier–Stokes (RANS) models. DNS is known to be the most computationally expensive and accurate method, and is capable of thoroughly interpreting turbulent eddies. However, the DNS method is noticeably time-consuming compared to other models. Acceptability of the RANS model has been debated throughout several studies; while some researches state that the k-ε and k-ω turbulence models are not suitable for capturing turbulent flows, evidence of the suitability of low-Re SST k-ω RANS model in accurately predicting inspiratory/expiratory flows has also been provided [27]. Other studies have been based on the laminar flow model, which possesses the advantage of time efficiency. However, it is not a suitable method for accurately capturing turbulent activities within airways, and is only used when the user is more interested in capturing non-turbulent aspects of fluid flows. In the simulations performed in the proposed study, the LES model was selected as a precaution against the occurrence of turbulent eddies that may potentially be induced by geometric influences [22,23]. It should be noted that future applications of the proposed model in various pathological analyses of airways flows involving turbulent flows, use of the LES simulation model seems appropriate.

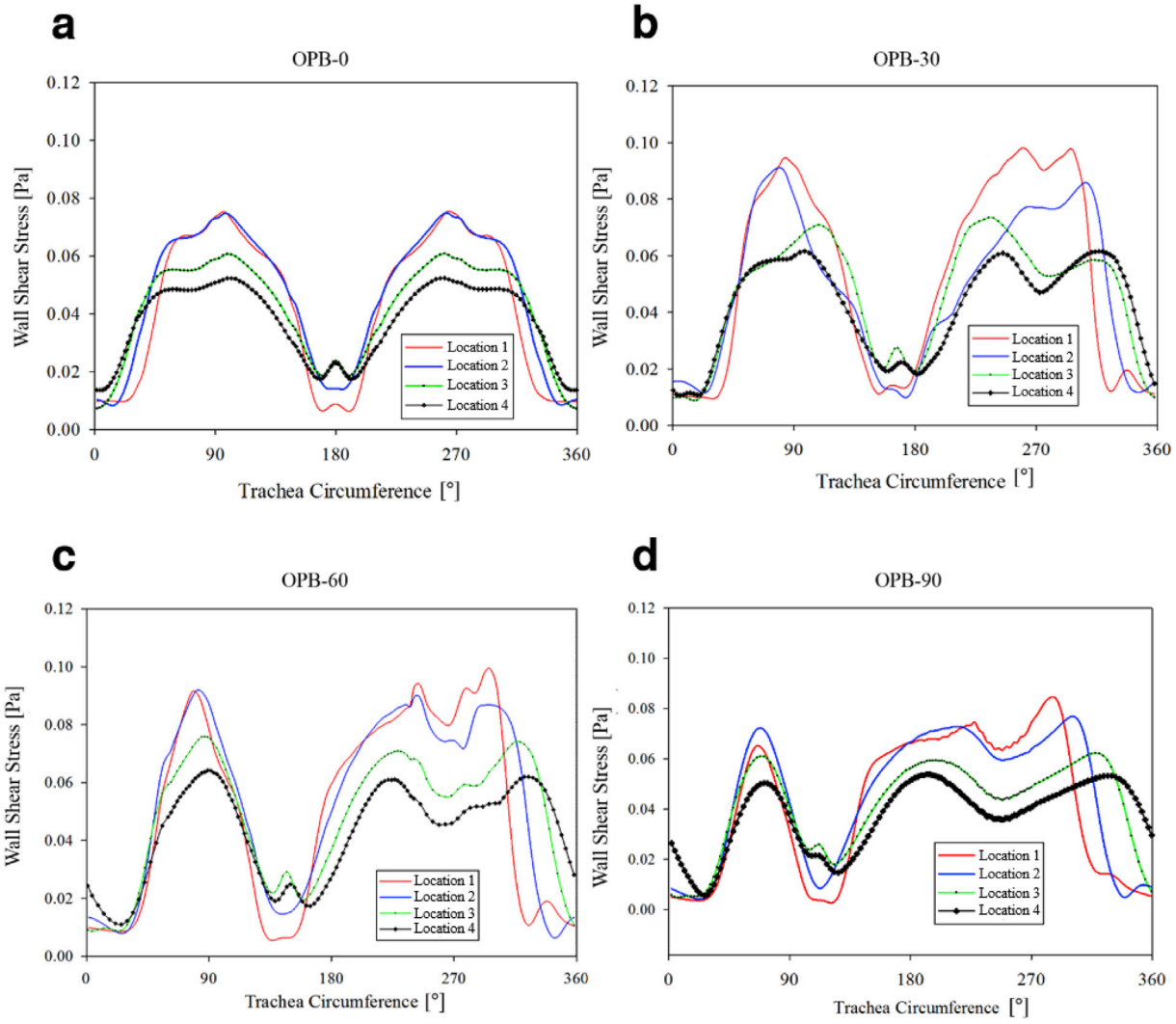

Fig. 8. Shear stress distributions on the tracheal wall exhibiting a shift based on asymmetric characteristics of OPB geometries. The trachea wall has been mapped onto a 360° circumferential x-axis graph. Locations 1–4 in the inset legends are equivalent to those in Figs. 1c or 6a. The graph is divided into the following four parts: The right wall (approximately 300°–40°), the anterior wall (40°–140°), the left wall (140°–200°), and the posterior wall (200°–300°). (a) The case with models constructed on symmetric bifurcation plane angles (OPB-0). The wall shear stress distribution is almost identical in the anterior and posterior regions. This is because the flow divides into two equal parts along the symmetric bifurcation plane. Additionally, (b, c, and d) denote shear stress distributions of the OPB-30, OPB-60, and OPB-90 models, respectively. The wall shear distribution displays a wider spread in the posterior region with increase in the bifurcation-plane angle. Furthermore, the peak level of the wall shear stress exceeds that observed in the OPB-0 model.

4.3. CFD boundary conditions and model selection

Selection of appropriate boundary conditions is essential in any CFD analysis. Generally, boundary-condition profiles may be defined by two methods. The first method involves application of pressure and velocity profiles at the inlet. The applied values are usually fixed or cyclic. A few examples include the usage of a parabolic fluid velocity inlet to generate a steady inhalation phase [28], a velocity profile defined on a grandmother branch [29], and a pressure inlet and constant pressure outlet [20]. The second method involves provision of a volumetric flow rate based on *a priori* knowledge [23,30,31]. In a few extant studies [32,33], clinical data on breathing patterns have been analyzed and proven to enhance the quality of CFD simulations. In the computational model used in the present study, a constant velocity boundary condition was defined at the inlet, and a constant pressure condition was applied to the outlets. Velocity boundary conditions matching the results obtained from experiments were defined to induce a constant-velocity flow. The MRB model proposed by Farkas and Balashazy [6] was selected as the basis of the OPB model, since it provided accurate measurements and parametrical data.

4.4. Limitations

For the sake of simplicity and clarity, 3 basic assumptions differing actual physiological phenomena were applied. However, these assumptions helped to more clearly demonstrate the fluid dynamic effects induced by off-plane bifurcation airway geometries. As the first approximation, the physiological transient expiratory flow was ignored; instead, steady-state flow was assumed. Secondly, airway wall compliant motion was not considered, and lastly, geometrical intricacies of the airway [34], including the flat posterior side of the lumen of trachea, corrugated tracheal walls owing to cartilaginous rings of the trachea, and slight bend in geometry in the longitudinal direction, were not included. Future studies will be performed to increase the accuracy of flow estimation by adding these physiological characteristics to the proposed computational model.

The off-plane bifurcation geometries employed in the proposed study involve samples of extreme cases, such as OPB-90. Although the possibility the off-plane bifurcation angle at the main carina of the trachea to exactly match the corresponding value of the proposed models is extremely small, an inspection of CT scans of abnormal airway patients

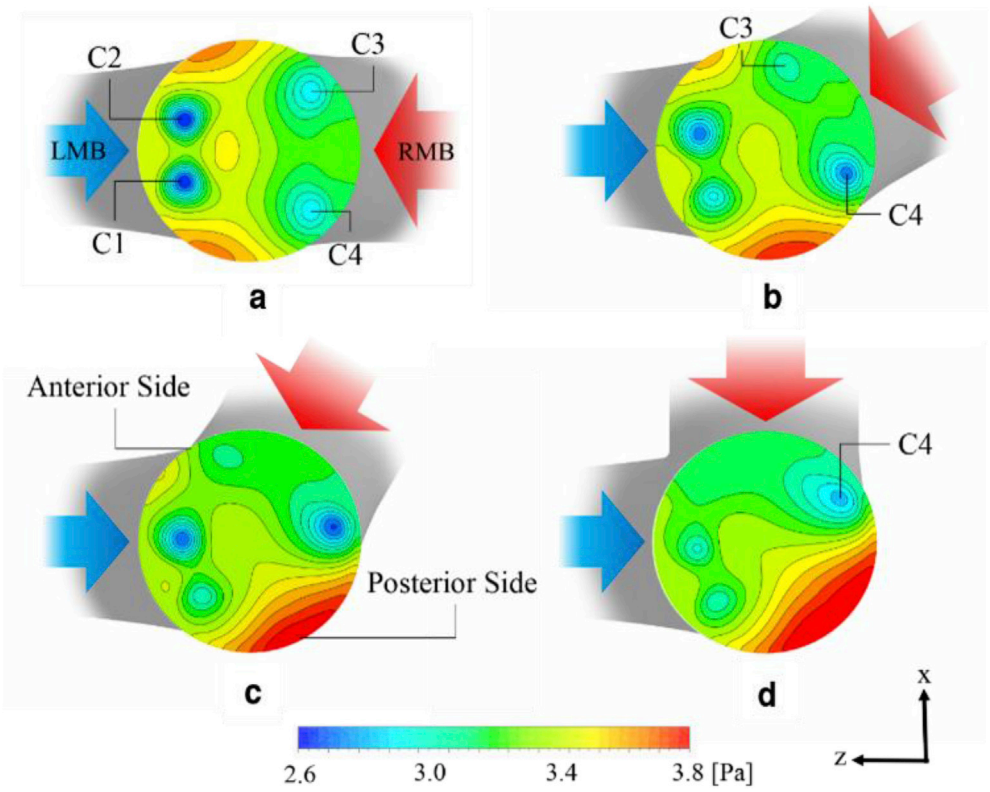

Fig. 9. Pressure distribution contour of OPB models. The pressure distribution of the merging flow in the observation point 1 (Fig. 3) is visualized. The blue arrows indicate the flow entering from the left main bronchus (LMB), and the red arrow represents the flow entering from the right main bronchus (RMB). The physical interpretation of the Bernoulli's principle is used to understand the manner in which the pressure distribution initiates the formation of the vortex cores. (a) The OPB-0 model shows the manner in which the pressure distribution focuses in relatively equal proportions with a slight bias to the left. The vortex cores (C1–C4) are visualized in the planes. Additionally, C1 and C2 are more developed (or stronger) because pressure distribution is higher in the left anterior and posterior walls. Moreover, (b–d) represent the OPB-30, OPB-60, OPB-90 models respectively, and show that the flow is concentrated in the posterior wall when the bifurcation angles become out-of-plane. When the pressure distribution of the right-posterior wall increases, the strength of the vortex core in that (C4) increases. (For interpretation of the references to color in this figure legend, the reader is referred to the Web version of this article.)

verifies that these cases exist and therefore, must not be discarded (Fig. S3). The proposed study, therefore, involved selection of four target models which were performed to determine their respective flow characteristics, thereby gaining a better understanding of human expiratory flows.

The proposed study does not examine the influence of branching generations that exceed the main bronchi. However, the MRB model [6] was selected to compare corresponding results with the OPB-0 model, and a discrepancy of 1.69% in terms of maximum velocity (Fig. S4) was observed. Furthermore, the angular positioning (formation) of vortex cores demonstrated flow characteristics that were in good agreement with the hypothesis reported in the earlier sections of this manuscript.

Lastly, the models proposed in this study comprised the trachea and bronchus separated by a fixed angle, which varies from person to person, to focus on the effect of off-plane bifurcation angles. It will be a very useful study to observe correlated effects of on- and off-plane angles between the trachea and bronchus on the resultant flow field inside the airway. The authors intend to take this up as a future endeavor.

5. Conclusion

A fully asymmetric model with complete 3D off-plane features of the airway geometry was examined numerically as well as via experiments. Six locations in the trachea were observed to characterize the flow pattern generated by the three-dimensionalities of the main bronchus angles. For all models, Dean-type secondary flow vortex cores were observed to be formed in a peculiar pattern in order to match the angle between the two main bronchi. However, increased concentration of imbalanced flow within off-plane geometries was observed to influence the flow field, thereby generating a counter-clockwise swerving motion as the flow elevated towards the trachea inlet. In addition, dominant cores were observed to have developed within off-plane models. The vortex core C4 exhibited the highest degree of distinctiveness in each model, with the exception of the symmetric model (OPB-0), owing to the concentrated flow generated on the right-posterior side of the trachea. Accordingly, shear stress distributions demonstrated significant changes when converted to off-plane angles.

Results of the proposed study indicate the impact of off-plane bifurcated airway geometries on expiratory flows inside human airways, and verify that symmetric models are limited in terms of capturing full flow characteristics inside human airways. There, however, exist differences between human airways across individuals, and thus, a more patient-specific model is necessary to obtain a better understanding of respiratory flows. It is expected that the present study in conjunction with extant studies that constitute a frontier in this field would aid and guide future research on respiratory diseases, such as tracheal distortion (stenosis), wounds inflicted by inflammation, and chronic obstructive pulmonary symptoms. It is suggested that studies must examine shear-stress characteristics on airway cells influenced by 3D flows. It is, however, important to verify whether shear stresses that occur in off-plane models affect the behavior of the tracheal epithelium in order to aid studies related to stenosis or inflammation-related air diseases [35,36]. In order to achieve a more physiologically realistic airway model, the authors propose to include two major *in vivo* features of airways—compliant motion of airway walls and pulsatile inhalation–exhalation breathing pattern— within the present model.

Conflicts of interests

The authors declare that there are no conflicts of interest.

Acknowledgments

This study was supported by a grant by the Korea Health Technology R&D Project through the Korea Health Industry Development Institute (KHIDI), funded by the Ministry of Health and Welfare (HI14C0559), and also supported by the Basic Science Research Program through the National Research Foundation of Korea (NRF), funded by the Ministry of Science, ICT and Future Planning (NRF- 2016R1D1A1B03934418). The authors thankfully acknowledge Prof. Jung Chan Lee from the Seoul

National University for his helpful discussions on respiratory system.

Appendix A. Supplementary data

Supplementary data related to this article can be found at https://doi.org/10.1016/j.compbiomed.2018.01.014.

References

[1] M.H. Tawhai, C.L. Lin, Airway gas flow, Comp. Physiol. 1 (2011) 1135–1157.
[2] V.K. Sidhaye, K.S. Schweitzer, M.J. Caterina, L. Shimoda, L.S. King, Shear stress regulates aquaporin-5 and airway epithelial barrier function, Proc. Natl. Acad. Sci. U. S. A. 105 (2008) 3345–3350.
[3] C.S. Kim, D.M. Fisher, Deposition characteristics of aerosol particles in sequentially bifurcating airway models, Aerosol Sci. Technol. 31 (1999) 198–220.
[4] Y. Zhao, B.B. Lieber, Steady inspiratory flow in a model symmetric bifurcation, Trans. ASME-K-J. Biomech. Eng. 116 (1994) 488–496.
[5] A. Green, Modelling of peak-flow wall shear stress in major airways of the lung, J. Biomech. 37 (2004) 661–667.
[6] Á. Farkas, I. Balásházy, Quantification of particle deposition in asymmetrical tracheobronchial model geometry, Comput. Biol. Med. 38 (2008) 508–518.
[7] C. Kleinstreuer, Z. Zhang, An adjustable triple-bifurcation unit model for air-particle flow simulations in human tracheobronchial airways, J. Biomech. Eng. 131 (2009) 021007.
[8] L.T. Holbrook, P.W. Longest, Validating CFD predictions of highly localized aerosol deposition in airway models: in vitro data and effects of surface properties, J. Aerosol Sci. 59 (2013) 6–21.
[9] D. Isabey, H. Chang, A model study of flow dynamics in human central airways. Part II: secondary flow velocities, Respir. Physiol. 49 (1982) 97–113.
[10] E.R. Weibel, Morphometry of the Human Lung, Springer, 1965.
[11] K. Horsfield, G. Dart, D.E. Olson, G.F. Filley, G. Cumming, Models of the human bronchial tree, J. Appl. Physiol. 31 (1971) 207–217.
[12] Y. Liu, R. So, C. Zhang, Modeling the bifurcating flow in a human lung airway, J. Biomech. 35 (2002) 465–473.
[13] T. Heistracher, W. Hofmann, Physiologically realistic models of bronchial airway bifurcations, J. Aerosol Sci. 26 (1995) 497–509.
[14] O. Raabe, H.-C. Yeh, G. Schum, R.F. Phalen, Tracheobronchial Geometry: Human, Dog, Rat, Hamster, 1976.
[15] U. Balásházy, W. Hofmann, Particle deposition in airway bifurcations—I. Inspiratory flow, J. Aerosol Sci. 24 (1993) 745–772.
[16] I. Balásházy, W. Hofmann, Particle deposition in airway bifurcations–II. Expiratory flow, J. Aerosol Sci. 24 (1993) 773–786.
[17] C.J. Hegedűs, I. Balásházy, A. Farkas, Detailed mathematical description of the geometry of airway bifurcations, Respir. Physiol. Neurobiol. 141 (2004) 99–114.
[18] T. Gemci, V. Ponyavin, Y. Chen, H. Chen, R. Collins, Computational model of airflow in upper 17 generations of human respiratory tract, J. Biomech. 41 (2008) 2047–2054.
[19] R.K. Freitas, W. Schröder, Numerical investigation of the three-dimensional flow in a human lung model, J. Biomech. 41 (2008) 2446–2457.
[20] N. Nowak, P.P. Kakade, A.V. Annapragada, Computational fluid dynamics simulation of airflow and aerosol deposition in human lungs, Ann. Biomed. Eng. 31 (2003) 374–390.
[21] X. Wu, P. Moin, A direct numerical simulation study on the mean velocity characteristics in turbulent pipe flow, J. Fluid Mech. 608 (2008) 81–112.
[22] T. Gemci, V. Ponyavin, Y. Chen, H. Chen, R. Collins, Computational model of airflow in upper 17 generations of human respiratory tract, J. Biomech. 41 (2008) 2047–2054.
[23] C.-L. Lin, M.H. Tawhai, G. McLennan, E.A. Hoffman, Characteristics of the turbulent laryngeal jet and its effect on airflow in the human intra-thoracic airways, Respir. Physiol. Neurobiol. 157 (2007) 295–309.
[24] W. Dean, J. Hurst, Note on the motion of fluid in a curved pipe, Mathematika 6 (1959) 77–85.
[25] I. Fluent, Fluent 6.3 Users Guide, Fluent Documentation, 2006.
[26] J. Zhou, R.J. Adrian, S. Balachandar, T. Kendall, Mechanisms for generating coherent packets of hairpin vortices in channel flow, J. Fluid Mech. 387 (1999) 353–396.
[27] J. Elcner, F. Lizal, J. Jedelsky, M. Jicha, M. Chovancova, Numerical investigation of inspiratory airflow in a realistic model of the human tracheobronchial airways and a comparison with experimental results, Biomechanics Model. Mechanobiol. 15 (2016) 447–469.
[28] J. Comer, C. Kleinstreuer, Z. Zhang, Flow structures and particle deposition patterns in double-bifurcation airway models. Part 1. Air flow fields, J. Fluid Mech. 435 (2001) 25–54.
[29] H. Luo, Y. Liu, Modeling the bifurcating flow in a CT-scanned human lung airway, J. Biomech. 41 (2008) 2681–2688.
[30] I. Balásházy, T. Heistracher, W. Hofmann, Air flow and particle deposition patterns in bronchial airway bifurcations: the effect of different CFD models and bifurcation geometries, J. Aerosol Med. 9 (1996) 287–301.
[31] C. Van Ertbruggen, C. Hirsch, M. Paiva, Anatomically based three-dimensional model of airways to simulate flow and particle transport using computational fluid dynamics, J. Appl. Physiol. 98 (2005) 970–980.
[32] J.K. Gupta, C.H. Lin, Q. Chen, Flow dynamics and characterization of a cough, Indoor Air 19 (2009) 517–525.
[33] J.K. Gupta, C.H. Lin, Q.Y. Chen, Characterizing exhaled airflow from breathing and talking, Indoor Air 20 (2010) 31–39.
[34] F. Lizal, J. Elcner, P.K. Hopke, J. Jedelsky, M. Jicha, Development of a realistic human airway model, Proc. Inst. Mech. Eng. H 226 (2012) 197–207.
[35] D. Huh, B.D. Matthews, A. Mammoto, M. Montoya-Zavala, H.Y. Hsin, D.E. Ingber, Reconstituting organ-level lung functions on a chip, Science 328 (2010) 1662–1668.
[36] J.E. Nichols, J.A. Niles, S.P. Vega, L.B. Argueta, A. Eastaway, J. Cortiella, Modeling the lung: design and development of tissue engineered macro-and micro-physiologic lung models for research use, Exp. Biol. Med. 239 (2014) 1135–1169.